



Article

Heat Waves and Human Well-Being in Madrid (Spain)

Domingo Rasilla ^{1,*} , Fernando Allende ², Alberto Martilli ³  and Felipe Fernández ²¹ Departamento de Geografía, Urbanismo y OT. Universidad de Cantabria, 39005 Santander, Spain² Departamento de Geografía, Universidad Autónoma de Madrid, 28049 Madrid, Spain; fernando.allende@uam.es (F.A.); felipe.fernandez@uam.es (F.F.)³ División de Contaminación Atmosférica, Centro Investigaciones Energéticas, Medioambientales y Tecnológicas, 28040 Madrid, Spain; alberto.martilli@ciemat.es

* Correspondence: domingo.rasilla@unican.es; Tel.: 34-942-206755

Received: 25 April 2019; Accepted: 14 May 2019; Published: 22 May 2019



Abstract: Heat waves pose additional risks to urban spaces because of the additional heat provided by urban heat islands (UHIs) as well as poorer air quality. Our study focuses on the analysis of UHIs, human thermal comfort, and air quality for the city of Madrid, Spain during heat waves. Heat wave periods are defined using the long-term records from the urban station Madrid-Retiro. Two types of UHI were studied: the canopy layer UHI (CLUHI) was evaluated using air temperature time-series from five meteorological stations; the surface UHI (SUHI) was derived from land surface temperature (LST) images from MODIS (Moderate Resolution Imaging Spectroradiometer) products. To assess human thermal comfort, the Physiological Equivalent Temperature (PET) index was applied. Air quality was analyzed from the records of two air quality networks. More frequent and longer heat waves have been observed since 1980; the nocturnal CLUHI and both the diurnal and nocturnal SUHI experience an intensification, which have led to an increasing number of tropical nights. Conversely, thermal stress is extreme by day in the city due to the lack of cooling by winds. Finally, air quality during heat waves deteriorates because of the higher than normal amount of particles arriving from Northern Africa.

Keywords: heat waves; urban heat island; heat stress; air quality; Madrid; Spain

1. Introduction

The warming of global temperatures during the last 150 years has been accompanied by an increase in the occurrence of heat waves [1,2], a trend that seems to be in close agreement with the most probable scenarios provided by climate models for the rest of the 21st century [3,4]. Heat wave impacts are diverse and widespread (crop failures, livestock losses, disruption of transportation, spreading of wildfires, power outages), but are particularly harmful in urban areas, due to the high population density and the urban heat island (UHI) effect, among other factors. UHI refers to a human-induced modification of the regional climate whereby the cities become warmer than their rural surroundings. Its magnitude is particularly intense at night, when an additional warming up to 7–10 °C have been recorded [5–7], although it can be reversed by day when the city becomes cooler than the surroundings [8]. Due to alterations in the natural landscape, urban environments absorb, preserve, and/or generate more heat, and gradually release heat compared with rural areas that cool off faster due to unobstructed outgoing radiation [9]. During heat waves, the prolongation of the diurnal thermal stress into the nocturnal hours deprives the population of relief, producing serious impacts on sensitive groups [10–13].

The Mediterranean area is widely recognized as one of the most vulnerable hot spots to climate change in the 21st century [14], particularly because of the predominance of the summer stable

atmospheric conditions, which are associated with heat waves and the build-up of pollutants, especially in larger urban areas [15]. Given the growing need to adapt to the consequences of global warming in a context of an aging population in the developed world, it is necessary to offer knowledge as detailed as possible about the space-time dynamics of this phenomenon and possible interactions with other urban phenomena, such as pollution, for its incorporation into studies about climate risks in urban spaces [16,17].

Studies of the spatial and temporal variability of temperature within urban spaces have relied on different methods [18,19]. UHI is usually quantified as the air temperature difference between the city and the corresponding air temperature of its surroundings (the canopy layer urban heat island, CLUHI). Urban networks are usually too sparse to provide detailed information about the intra-urban temperature variations, which can be resolved using remote sensing, which provides the surface urban heat island (SUHI). Satellite monitoring of extreme heat events in urban areas [20–22] has improved the knowledge about the spatial variability of this phenomenon. However, comparison between canopy and surface UHIs should be cautious because of their diverse dynamics [23].

The analysis of the impact of heat waves should include also the assessment of the human sensation of heat, quantified throughout the use of proper bioclimatological indices [24,25] which consider the whole heat balance of the human body, not only including the use of air temperature, but also additional variables such as air humidity, wind speed, as well as short- and long-wave radiation flux densities, in addition to human components like activity level or clothing type [26,27].

Air pollution further exacerbates the adverse effects of heat waves. Slow-moving high-pressure systems, the most common synoptic environment conducive to heat waves, are responsible for dry conditions, strong sunlight, and low wind speeds, allowing poor-quality air to stagnate in a given location for extended periods of time and accumulating pollutants [28–30]. These atmospheric conditions increase the emission of biogenic volatile organic compounds, which boost the production of surface ozone and other aerosols [31]. Drought-like conditions reduce soil moisture, making near-surface temperatures hotter and inhibiting the role played by vegetation in absorbing pollutants, resulting in worse air quality [32,33].

The objective of this study was to identify some characteristics of the heat waves (frequency, trends) that have been observed in Madrid since 1880 and to assess the urban heat island, thermal comfort, and air quality during those events.

2. Data and Methodology

The study area comprises the metropolitan area of Madrid, the capital of Spain. Madrid lies on the southern area of the Spanish Plateau, between the Jarama and Manzanares river basins, in the wider Tagus River catchment area. Orography is relatively rugged, since there are substantial differences in altitude, ranging from 846 m a.s.l. in the north to 543 m a.s.l. in the southeast. Due to its altitude and distance to the sea, the city experiences an extreme version of the Mediterranean climate, characterized by scarce precipitation, mostly in autumn and spring, and large annual and diurnal temperature changes. Summers are particularly warm (July average maximum temperature at Madrid-Retiro 32.1 °C) and dry (July 11 mm, August 9 mm), with most of the precipitation falling as convective showers.

Madrid is also the most populated urban area of Spain: 3.5 million people live in the municipality as of 2018, spread over 604.3 km², but the population of the whole metropolitan area is approximately 6.5 million. The city experienced vigorous growth from the beginning of the century to 1970, increasing from approximately 500,000 to 3 million people. After that, urbanization focused on the surrounding locations (Figure 1). Vulnerable population groups (e.g., the elderly and youngsters) represent 33.3% of the total, to which we must add people coming from other countries who can also be exposed to the heat, since Madrid has become a popular tourist destination [34]. There are 4,699,917 vehicles officially registered in the province of Madrid [35], 1,500,000 of which enter the core of the city every day [36].

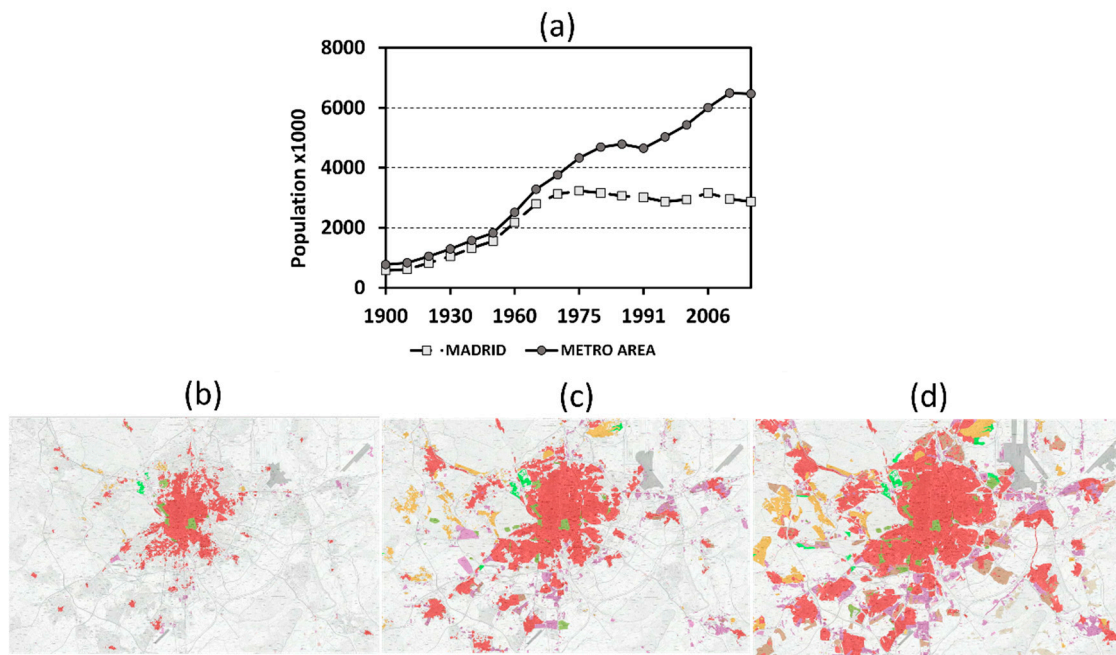


Figure 1. (a) Evolution of the population in Madrid and expansion of the urban land uses during the second half of the 20th century: (b) 1956 (c) 1980, and (d) 2005.

Data used in this research originated from various sources. Meteorological data (daily maximum and minimum temperature; temperature, relative humidity, wind speed, and cloudiness at 00, 07, 13 and 18 UTC) from synoptic weather stations were obtained from AeMet, the Spanish meteorological office (Table 1 and Figure 2). Specifically, the long-term trends in heat waves were analyzed on the time series of Madrid-Retiro weather station retrieved from the SDATS (Spanish Daily Adjusted Temperature Series) database [37]. The SDATS timeseries were homogenized and adjusted to solve some temperature inhomogeneities derived from the “screen bias” (change from Montsouris to Stevenson screen), changes in placement and an artificial warming trend between 1894 and 1960, the period of the largest population increase.

Seasonal composites of large-scale climatic variables (e.g., 500 hPa geopotential heights and 850 hPa temperature) were extracted from the NCEP/NCAR Reanalysis web site (<http://www.esrl.noaa.gov/psd/>).

Land surface temperature (LST) was analyzed using the product MYD11A1 (V6) -MODIS/Aqua Land Surface Temperature and Emissivity Daily L3 Global 1 km Grid SIN. Although the MODIS (Moderate Resolution Imaging Spectroradiometer) sensor is installed on two platforms, Aqua and Terra, only the first one was used because its approximate time of passage over the Iberian Peninsula (1:30 a.m. and 1:30 p.m.) is more suitable for the analysis of the surface UHI. Compared with other platforms (e.g., ASTER or LANDSAT), the lower spatial resolution ($\sim 1 \text{ km}^2$) is compensated for by a higher temporal resolution, which enables studying the temporal dimensions of the phenomenon. This product has already been used in research on surface UHI in cities of varying sizes and climates, for example in Europe [38,39] and Asia [40]. Previous studies confirmed the accuracy of the MODIS LST product, particularly by night under clear skies [41,42]. Additional technical details can be consulted on the NASA website (<https://lpdaac.usgs.gov/>). The original images were subjected to a basic quality control analysis using only those days with more than 90% valid pixels within the limits of the image (a total of 7,645 images). To relate the surface temperature to land uses, the MODIS images were cross-referenced with the Global Land Cover 2000 database [43]. This database covers the entire planet, providing 22 categories with a resolution of 1 km^2 , obtained from the VEGETATION sensor (SPOT 4 satellite). The types of land uses (Land Cover Classification System, LCCS) are inspired by the FAO (Food and Agriculture Organization).

Additionally, air quality data were retrieved from the local Ayuntamiento de Madrid [44] and regional Comunidad de Madrid [45] authorities. Long-term statistics of occurrence of Saharan outbreaks were downloaded from the Spanish Ministerio para la Transición Ecológica [46].

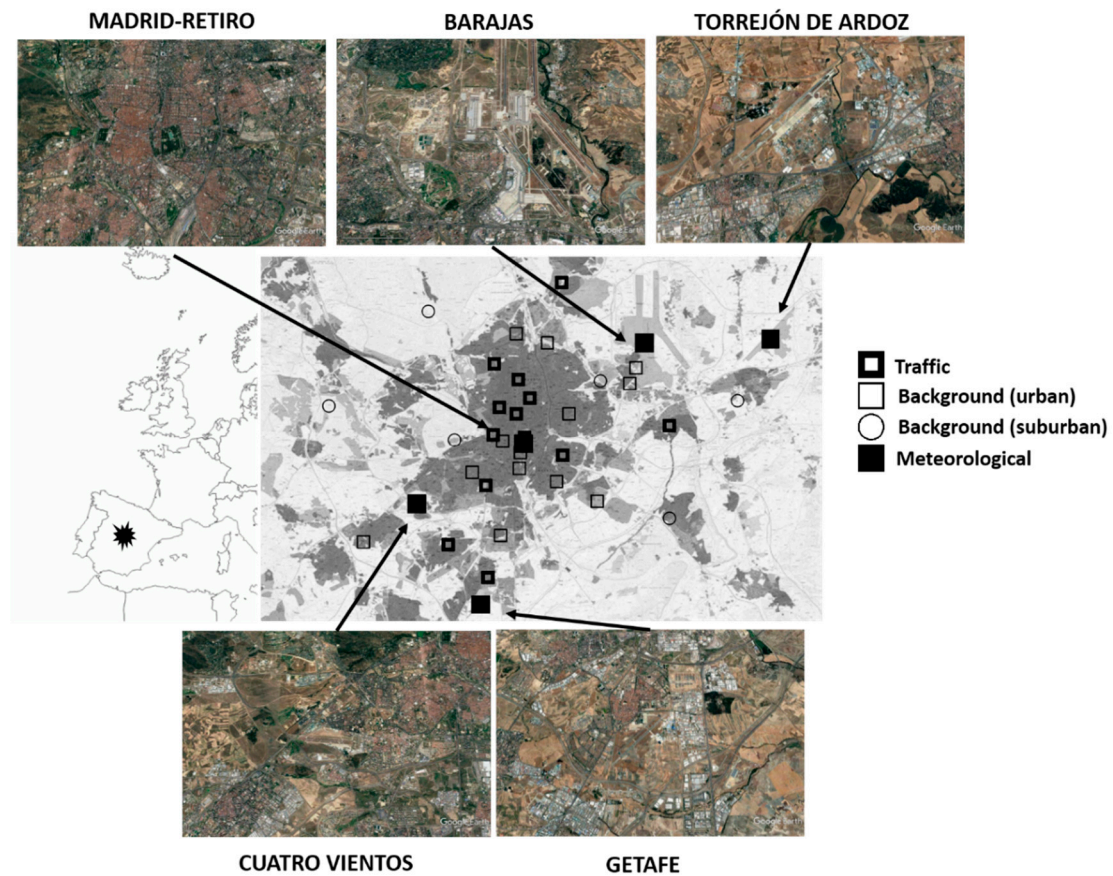


Figure 2. Location of the study area. Weather stations are depicted as filled squares (accompanied by an aerial view) and air quality stations as empty squares or circles, depending on their class.

Table 1. Location of the meteorological stations.

Station	WMO Code	Latitude	Longitude	Altitude	Period	LCZ ¹
Barajas	8221	40.494 N	3.567 E	609	1961–2017	8/D
Madrid-Retiro	8222	40.417 N	3.683 E	667	1880–2017	2/B
Cuatro Vientos	8223	40.371 N	3.785 E	691	1961–2017	5/D
Getafe	8224	40.294 N	3.724 E	618	1961–2017	6/D
Torrejón de Ardoz	8227	40.497 N	3.446 E	617	1961–2017	8/D

¹ Local Climate Zones [47].

Despite of the relevance of the phenomenon, no universal definition of a heat wave exists [48–50]. A heat wave can be considered as an extended period of hot days; from the statistical point of view, a hot day may be identified when air temperature rises beyond a threshold, usually calculated from the temperature distribution recorded at a meteorological station. Using this basic procedure, but considering the results of previous analyses of the impact of the high temperatures in Madrid [51–53], we identified those days in which the maximum temperature exceeds 36.5 °C at Madrid-Retiro as *extreme hot days* (EHD). This value is equivalent to the 95th percentile of the daily maximum summer (June, July, and August) temperature for the 1981–2010 period. Consequently, a heat wave was defined as a period of at least 3 consecutive EHDs, becoming *heat wave days* (HWDs). In case of an intermediate day between two heat waves, recording a maximum temperature below such threshold, but above

the 90th percentile, it was also considered an EHD and both heat waves were merged into a single heat wave.

The magnitude of the CLUHI was quantified as the air temperature difference (ΔT) between the urban (Madrid-Retiro) and any other non-urban stations, calculated for both maximum (daytime) and minimum (nighttime). A positive value indicates that Madrid-Retiro is warmer, whereas a negative value indicates that is cooler. The Local Climate Zones (as defined by Stewart and Oke [47]) for each station are presented in Table 1. Madrid-Retiro's station is located in a park (LCZ B), approximately 100 m from a dense urban area (LCZ2). Barajas is the weather station of the busiest airport in Spain, and it is located over a Low Plant (LCZ D) area, close to the main runway, with edifications (terminals) at distances of less than 500 m (LCZ8). Cuatro Vientos, Getafe, and Torrejón de Ardoz are other meteorological stations located at smaller airports, nearby urban areas of different densities. Also, the number of summer tropical nights ($T_{min} > 20\text{ }^{\circ}\text{C}$) [54] was calculated for the long-term evaluation of the nighttime heat conditions.

To describe and quantify heat waves from a human-biometeorological point of view, the Physiological Equivalent Temperature (PET) index was calculated by the RayMan model [55,56]. PET describes the effect of the thermal environment as a temperature value ($^{\circ}\text{C}$), which facilitates interpretation of the results, and is based on the full human energy balance. PET is equivalent to the air temperature at which, in a typical indoor setting, the heat balance of the human body (work metabolism, 80 W of light activity, added to basic metabolism; heat resistance of clothing, 0.9 clo) is maintained with core and skin temperatures equal to those of a body in the assessed conditions [57]. The classification of PET and the related physiological strain are given in Table 2.

Table 2. Physiological Equivalent Temperature (PET) for different grades of thermal sensation and physiological stress on human beings (during standard conditions: heat transfer resistance of clothing, 0.9 clo; internal heat production, 80 W) [58].

PET	Thermal Sensation	Physiological Stress Level
<4	Very cold	Extreme cold stress
8	Cold	Strong cold stress
13	Cool	Moderate cold stress
18	Slightly cool	Slight cold stress
23	Comfortable	No thermal stress
29	Slightly warm	Slight heat stress
35	Warm	Moderate heat stress
41	Hot	Strong heat stress
>41	Very hot	Extreme heat stress

To evaluate potential health risks for the population due to abnormal concentrations of air pollutants, daily averages, exceedances and ratios during normal days and HWD, plus a daily pollution index (PI), were calculated for selected pollutants (PM_{10} , NO_2 and O_3). The PI [59] defines five distinct air quality classes and matches a reference concentration (C_p) of each individual pollutant (either daily PM_{10} , maximum 8-hour O_3 , or maximum hourly NO_2 concentrations) to one of the five categories (Table 3). The PI is expressed by:

$$PI = \frac{PI_{hi} - PI_{lo}}{BP_{hi} - BP_{lo}}(C_p - BP_{lo}) + PI_{lo} \quad (1)$$

where BP_{hi} and BP_{lo} are the upper and lower concentration breakpoints of each PI category, respectively, to which C_p corresponds; and PI_{hi} and PI_{lo} are the upper and lower PI breakpoints of the same category, respectively (Table 3).

Table 3. Concentration breakpoints ($\mu\text{g}\cdot\text{m}^{-3}$) and corresponding pollution index (PI) values, for each PI air quality category [60].

Pollution Category	PI	PM ₁₀ 24-h Average ($\mu\text{g}\cdot\text{m}^{-3}$)	NO ₂ 24-h Max. ($\mu\text{g}\cdot\text{m}^{-3}$)	O ₃ 8-h Daily Max. ($\mu\text{g}\cdot\text{m}^{-3}$)
Unhealthy	100	500	1900	500
Unhealthy for sensitive groups	85	238	950	223
Moderate pollution	70	144	400	180
Low pollution	50	50	200	120
Good quality	25	20	40	65

The chi-square test of independence was used to evaluate whether a significant association exists between the categories of two dichotomous variables, HWD and Saharan outbreaks (days). It is a non-parametric (distribution free) test designed to analyze group differences, being robust with respect to the data distribution. Specifically, it does not require equality of variances among the study groups nor homoscedasticity in the data.

3. Results

In this section, we first review the main temporal characteristics of heat waves in the Madrid metropolitan area to continue with an analysis of how heat waves affect the UHI phenomenon. Finally, we show the impact of heat waves on the air quality conditions.

3.1. Long-Term Trends on Heat Waves Occurrence

Figure 3 shows the summer (JJA) average maximum temperature, the corresponding absolute maximum temperature, and the number of EHD per summer season between 1880 and 2017 at Madrid-Retiro. Years prior to 1880 were disregarded because of doubts about the data quality. The evolution of both absolute and average maximum temperatures display large inter-annual variability, but decadal trends are clearly connected with well-known phases of global temperatures. Both parameters show a warming phase between 1880 and 1933 ($0.03\text{ }^{\circ}\text{C}\cdot\text{year}^{-1}$), replaced by a cooling trend up to 1979 ($-0.04\text{ }^{\circ}\text{C}\cdot\text{year}^{-1}$). The last four decades of the 20th century exhibit a strong and continuous warming trend, which amounts $0.09\text{ }^{\circ}\text{C}\cdot\text{year}^{-1}$. Overall, since 1880, the average maximum temperature at Madrid-Retiro shows a warming trend of $0.03\text{ }^{\circ}\text{C}\cdot\text{year}^{-1}$. The warmest year was 2016, with an average maximum temperature of $33.4\text{ }^{\circ}\text{C}$. On a decadal time scale, the 10-year period between 2008 and 2017 must be considered the warmest in the historical record ($32.1\text{ }^{\circ}\text{C}$; $\Delta T = 1.6\text{ }^{\circ}\text{C}$ with regard to the 1981–2010 “normal” period). The trend observed in the absolute summer maximum temperature is similar to the average maximum temperature, although the variability is larger since it depends on the occurrence of single day events. Two summers (2012 and 2017) out of three recorded an absolute maximum temperature higher than $40\text{ }^{\circ}\text{C}$ in the aforementioned 10-year period since 2009.

Another important feature of Madrid’s recent summer climate is the increase in the frequency of EHD after the 1980s, which has occurred in longer spells (Figure 4a). Before 1980, occurrences of EHD was a rare phenomenon, most of the time as single- or two-day events. The most remarkable summer was 1949, which experienced both a four-day and a three-day event; however, 18 summers (60%) between the 1948 and 1979 recorded no heat wave. The situation reversed after 1979, as a clear increasing trend is detected; the slope of the linear fit equals 0.27 more HWD per year. We found that 2015 emerged as the absolute record year in the frequency of HWD, with 24 days, followed by 2017, with 20 days, and 1991 with 17 days.

Derived from the increase in the number of HWD and the length of the episodes, the core of the summer, spanning from July 16 to August 15 (traditionally known as “canícula”) has extended, particularly to June [60,61]. Most of the HWD until the 1980s were observed in July (74%) and August (22%); the earliest HWD occurred on June 29 (1950) and the latest on August 17 (1949). During the last four decades, summer is uniformly hotter than before, and the period prone to heat waves extends

to June (13%) and August (22%); the earliest have been recorded on 11 June 2017 and the latest on 29 August 2009.

Regarding the possible causes of the warming experienced since the 1980s, Figure 4b shows the daily maximum temperature distribution function corresponding to almost equally long temporal periods, 1948–1979 and 1980–2017. Visually, both distributions are quite similar, but the mean and the median of the second period are displaced almost 1.5 °C to the right. This shift suggests the impact of the global trend to higher temperatures on the aforementioned warming.

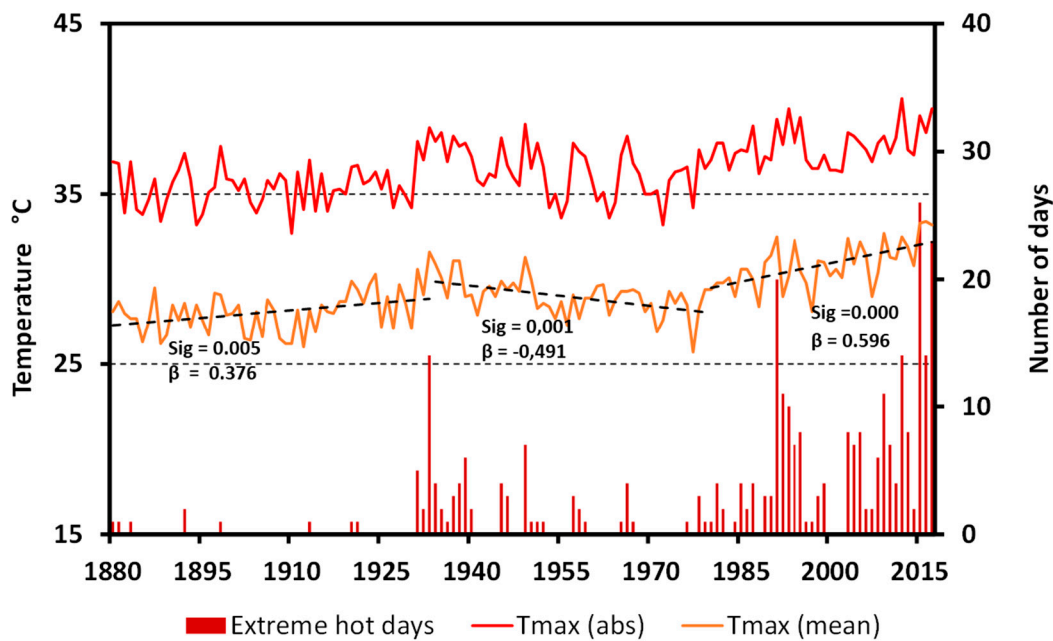


Figure 3. Temporal evolution (1880–2017) of the summer (JJA) average maximum temperature, absolute maximum temperature and the number of extreme hot days (EHD). Linear trends of average maximum temperatures are featured according to three sub-periods (1880–1933, 1934–1979, and 1980–2017).

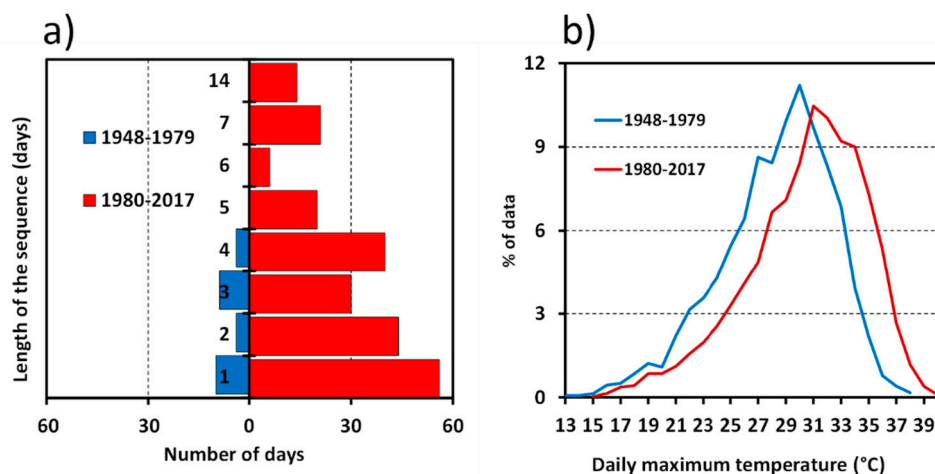


Figure 4. (a) Length runs of EHDs and (b) summer (JJA) daily maximum temperature distribution corresponding to the periods 1948–1979 and 1980–2017 at Madrid-Retiro.

However, a regional component of this summer warming may exist. Figure 5a displays the anomalous pattern of 500 hPa geopotential heights, composited from the 1980–2017 period minus the 1948–1979 period. The positive area over the Western Mediterranean Basin is consistent with the

observed warming trend of maximum temperatures, since the large-scale pattern should induce a broad-scale subsidence and adiabatic compression upon the tropospheric air masses.

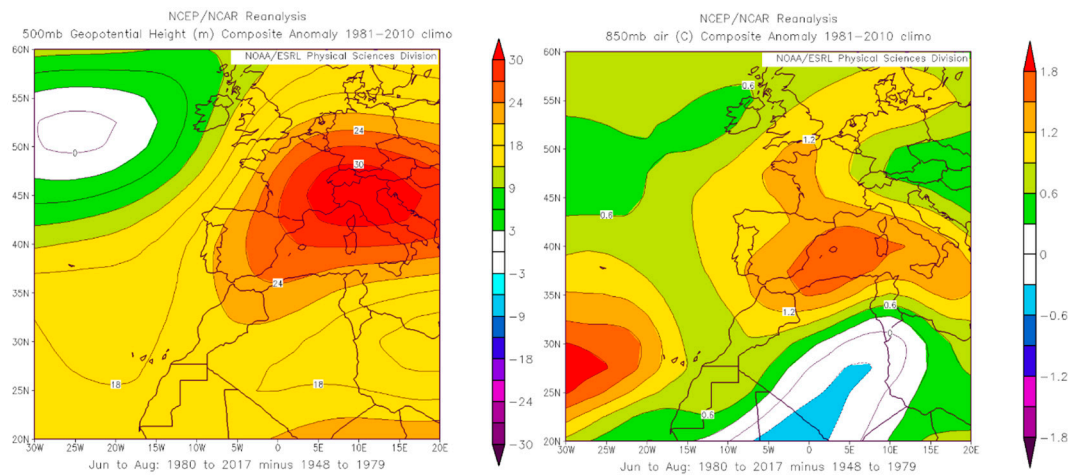


Figure 5. Composite anomaly maps of (a) 500 hPa geopotential heights (mts) and (b) 850 hPa temperature (°C), corresponding to the period 1980–2017 minus 1948–1979 (from NCEP/NCAR reanalysis database).

The pattern displayed in Figure 5a ensures an upper-level southerly flux with negative relative vorticity and a warm advection over the studied area, probably of Saharan origin, as portrayed by the 850 hPa temperature field (Figure 5b). The polar plots depicting the bivariate relationship between 13 UTC summer air temperature at Retiro and simultaneous surface wind and 850 hPa records from Barajas airport (Figure 6) emphasize the southerly component of the wind, more evident at the surface due to the orientation of the Jarama valley, where the airport facilities are located.

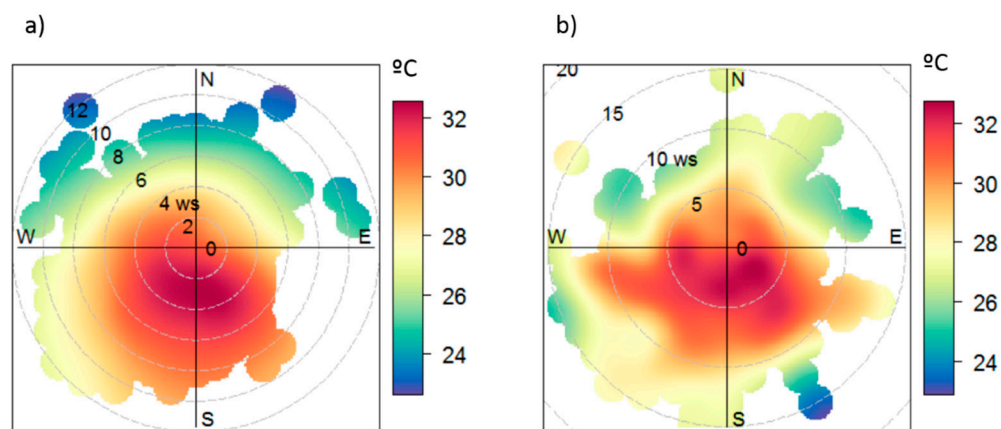


Figure 6. Polar plots relating 13 UTC summer air temperature records at Retiro and simultaneous (a) surface and (b) 850hPa wind records from Madrid-Barajas airport.

3.2. Heat Waves and UHI

3.2.1. CLUHI

Due to the aforementioned increased frequency of heat waves after 1980, we relied upon the period 1980–2017 for the analysis of the impact of those events upon Madrid’s summer CLUHI, which is a frequent phenomenon by night, as a response of its large urban size and predominance of stable atmospheric conditions. Positive differences in minimum temperatures at Madrid-Retiro occur almost 9 of each 10 nights, with average differences up to 2.5 °C and maximums up to 5.5 °C (Figure 7). Distance to the city center and topography explain the primacy of Torrejón de Ardoz (LCZ2/B vs.

LCZ8/D difference). Barajas (also a LCZ2/B vs. LCZ8/D difference) experiences similar but less intense differences, probably because the station is surrounded by the facilities of the busiest airport in Spain. Cuatro Vientos and Getafe (LCZ2/B vs. LCZ5/D, and LCZ2/B vs. LCZ6/D differences, respectively), display weaker differences in response to their suburban and southward locations, and less favorable topography to nocturnal cooling. By day, urban-to-rural differences reverse for all stations.

Heat waves enhance the nocturnal temperature contrast by night. The average minimum temperature difference between Madrid-Retiro and Torrejón de Ardoz rises from 2.9 °C during normal conditions to 3.4 °C during heat waves; for Barajas, the corresponding values are 1.9 °C and 2.6 °C. Conversely, no differences are observed at Cuatro Vientos and Getafe. By day, no substantial differences are observed during heat waves.

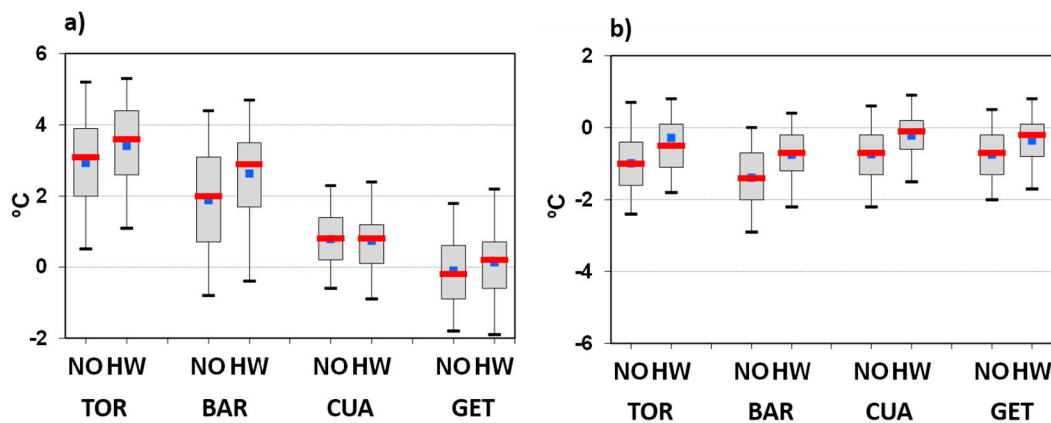


Figure 7. Statistical distribution of the air temperature difference between Madrid-Retiro and each other observatory for daily (a) minimum and (b) maximum temperature during normal summer days and HWD for the 1980–2017 period. TOR stands for Torrejón de Ardoz, BAR for Barajas, CUA for Cuatro Vientos and GET for Getafe. Grey boxes account for the lower (25%) and upper (75%) quartiles, red rectangles represent the median, blue dots the average, and whiskers indicate the value of the 5% and 95% percentiles.

As a direct consequence of the generalized warming, the number of summer tropical nights has increased since 1961 across the region, but the trend is faster in Madrid-Retiro (0.56 days per year) than in Torrejón de Ardoz (0.26 days per year) because of the intensification of nocturnal urban warming (Figure 8). Both trends are statistically significant at a probability level of 0.001 according to a *t*-test.

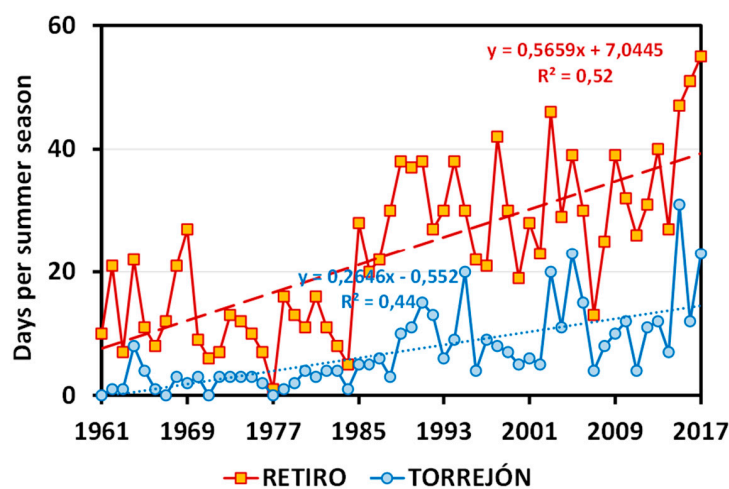


Figure 8. Long-term trends in the number of summer (JJA) tropical nights (daily minimum temperature > 20 °C) at Madrid-Retiro and Torrejón de Ardoz.

3.2.2. SUHI

The response of the earth surface to the atmospheric conditions created by heat waves follows the same direction observed in the case of air temperatures. Figure 9 displays the spatial pattern of average LST corresponding to the nocturnal and diurnal images during HWD, and their pixel-to-pixel differences with respect to normal summer conditions, obtained for the 2002–2017 period.

As a whole, the maps indicate that surface temperature anomalies coincide, to a great extent, with the built environment. The more irregular diurnal spatial pattern during daytime contrasts with the concentric disposition of the surface temperature field by night, when the center of Madrid is surrounded by an archipelago of smaller heat islands. By day, shadows and the greater heat capacity of urban materials explain the slower warming of the city, forming a surface urban “cool” island (SUCI). The lowest temperatures are visible at the western border of the city, in connection with the valley of the Manzanares river and the urban forest of Casa de Campo (about 10 °C less than the warmest spots). At the southeast, the warmest anomalies appear due to the presence of bare soils under gypsum rocks, accompanied by some isolated cool spots that coincide with wet surfaces (Jarama river). At night, the slow release of the heat accumulated in the city keeps the city warmer (about 24 °C) than the surroundings. Several lines, following the transportation system, join Madrid with the smaller suburban cities, like Móstoles and Getafe, whose islands are weaker (about 22 °C). The Barajas airport complex, in the north, becomes one of the coolest spots, as well as the valleys of the Manzanares (NW) and Jarama (SE) rivers, highlighting the role of the topography in channeling cool air masses from the surrounding mountains and plateaus.

The map of nighttime anomalies confirms that, as with air temperature, SUHI intensifies during heat waves. The area corresponding to the highest anomalies is displaced to the more northerly neighborhoods of Madrid, which are also characterized by a high build-up density and narrow streets, but smaller urban nuclei also show positive anomalies of LST. Negative anomalies show a longitudinal N–S arrangement, which roughly corresponds to the background of the valleys of the Manzanares (to the west) and Jarama (to the east) rivers. By daytime, heat waves intensify the SUCI, by increasing LST at two particular locations: the NW and the SE.

To properly quantify the impact of the different land uses on surface temperature due to heat waves, we calculated the average LST values pixel-by-pixel, and then we grouped them together according to several categories (Figure 10). According to the Global Land Cover 2000 database, urban uses represent approximately 14% of each image, woodlands 9.1%, rain fed crops 67.1%, and scrub/grassland 9.8% (for sake of simplicity, the two latter were grouped together into a class named herbaceous).

The thermal diversity is higher by day as a result of the multiple reflections of solar radiation associated with the sun’s path over the horizon, the larger albedo values, and the shadows generated by buildings or the presence of vegetation within urban areas, in contrast to a constant emission of infrared radiation by night. Urban spaces are confirmed to be areas with lower thermal amplitude, cooler by day (46.9 °C) and warmer by night (23.1 °C). The type of vegetation also controls the values of LST by daytime (forests being the coolest), although the differences diminish by night.

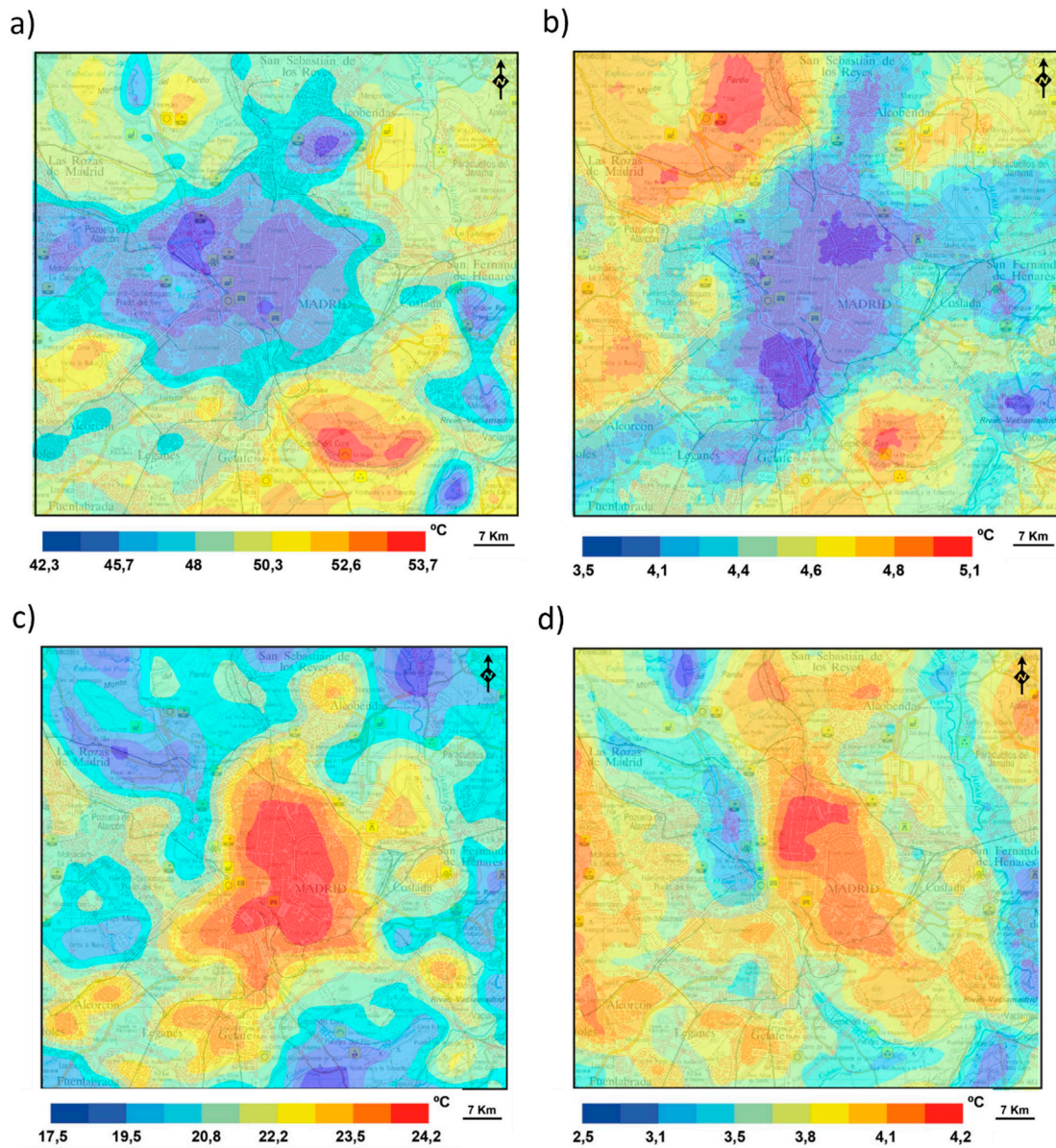


Figure 9. Spatial pattern of summer (a) daytime and (c) nighttime LST during HWDs and difference with respect to (b) days and (d) nights without heat waves.

The arrival of hot air masses during heat waves produces a general increase in LST at any time. Comparing the temperature of urban surfaces with the other land uses, we found that the enhancement of the diurnal “cool” island is slightly larger (-1.5 °C normal days, -2.1 °C heat wave days) than the nocturnal heat island (2 °C versus 2.3 °C , respectively) because of the greater temperature increase of forest and herbaceous surfaces.

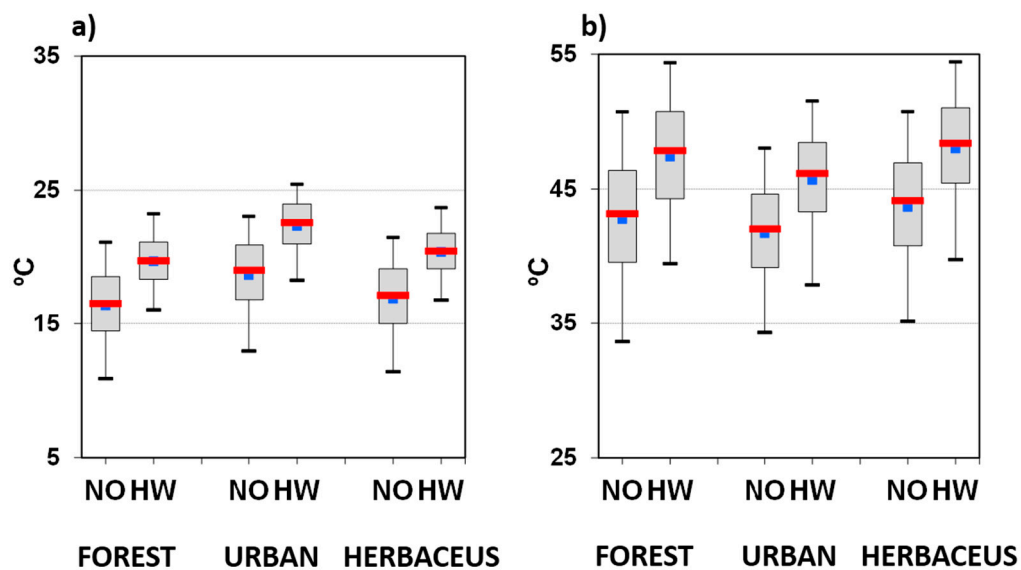


Figure 10. Statistical distribution of LST by land uses for (a) nighttime and (b) daytime during normal summer days (NO) and heat wave days (HWD). Grey boxes account for the lower (25%) and upper (75%) quartiles, red rectangles represent the median, blue dots the average, and whiskers indicate the value of the 5% and 95% percentiles.

3.2.3. Physiologic Urban Heat Island

Urban comfort conditions were assessed at each meteorological observatory using PET values, also calculated for the 1980–2017 period. Figure 11 presents the frequency of occurrence of each PET classes during normal days and HWD, during both nighttime and daytime. A clear shift to higher PET classes is depicted during HWD, particularly during daytime. The figure also reveals that the distribution of PET classes on each observatory is in accordance with the distance to the city center. As expected, the population suffers very hot conditions during most of the HWD days at 13 UTC, particularly those living in the city center (almost 100% of the days); very hot conditions were also common in Cuatro Vientos and Getafe, as the former weather station also experiences a weaker UHI and the latter occupies a southward location. Night hours provide relief of the heat stress, since comfortable sensations are predominant; however, slightly warm conditions are present in urban observatories, whereas slightly cool conditions characterize nights in the outskirts of Madrid.

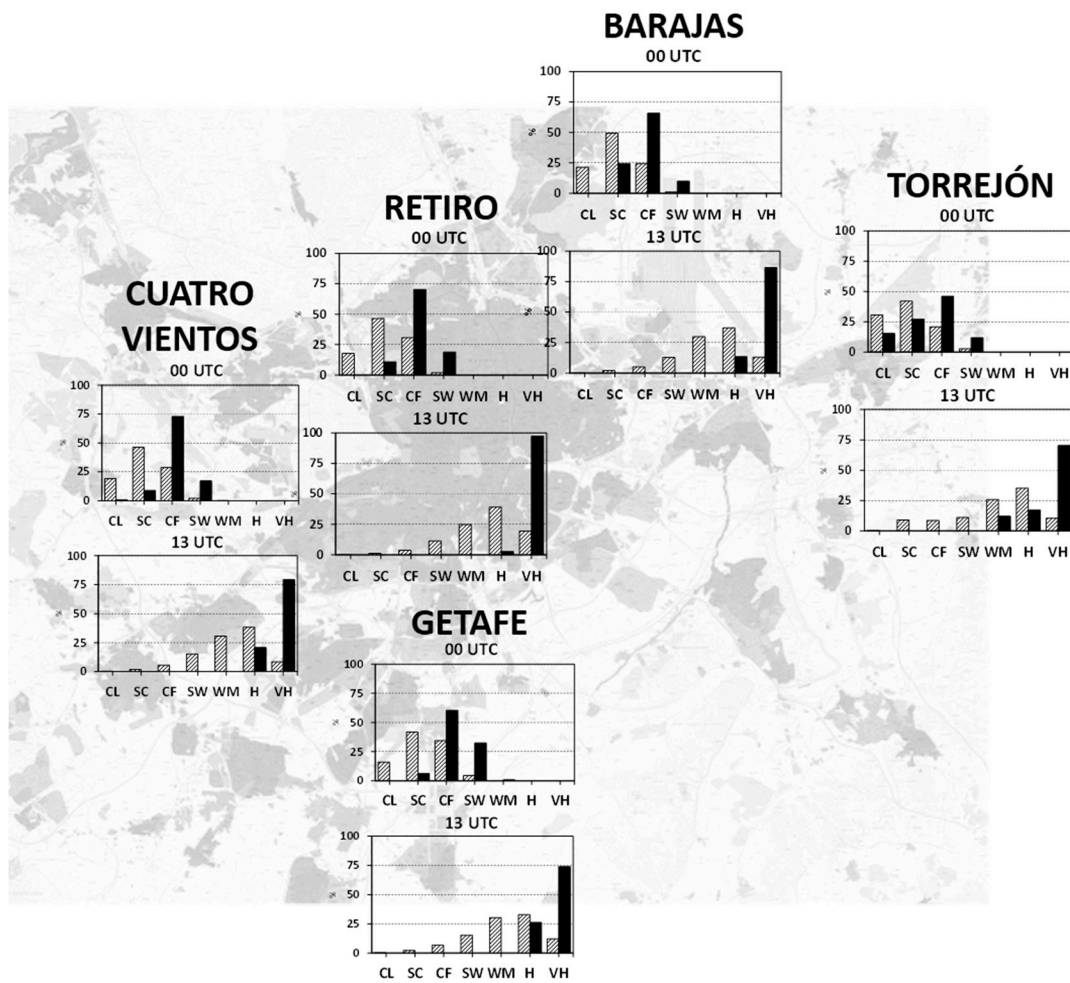


Figure 11. Frequency of occurrence of PET classes by nighttime (00 UTC) and daytime (13 UTC). (VH: Very Hot; H: Hot; WM: Warm; SW: Slightly Warm; CF: Comfortable; SC: Slightly Cool; CL: Cool) during normal days (hatched bars) and HWD (black bars).

3.3. Air Quality During Heat Waves

The mean pollution levels during HWD and their ratios (% of variation) regarding normal days for selected pollutants are presented in Figure 12. The mean concentration of all pollutants increased during HWD, but the increase was significant in most stations only for PM₁₀ levels according to a *t*-test. The increases in NO₂ levels were less pronounced, and non-relevant for O₃ levels. The higher increases of PM₁₀ concentration (sometimes more than 60%) were observed at stations inside the city, rather than in suburban places (less than 25% on average), mainly at the NE, which might be a consequence of the displacement of the urban plume by the southerly winds during HWD. As stated previously, the moderate increase in NO₂ concentrations showed no clear spatial pattern.

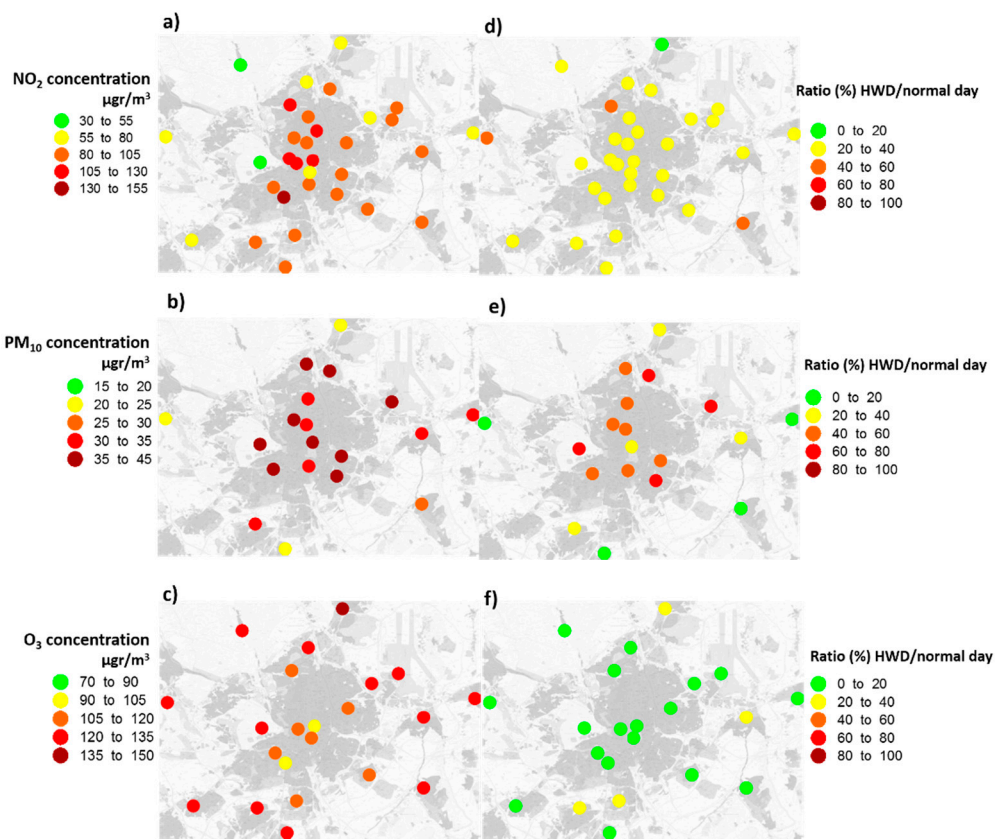


Figure 12. Spatial patterns of summer (JJA) daily average concentrations of NO₂ (upper row), PM₁₀ (middle row), and O₃ (lower row) corresponding to HWD (left column) and the ratio between HWD and normal summer days (right column).

As expected, the increase in the average concentration levels during HWD resulted in the air quality standards being exceeded. Figure 13 shows the probability of occurrence of a PM₁₀ exceedance (more than 50 µg m⁻³) during HWDs with respect to normal days. This dimensionless value was calculated by dividing the probability of a PM₁₀ exceedance occurrence during a HWD by the probability of an exceedance occurrence during a normal summer day (probability of occurrence of an exceedance calculated as number of days with exceedances by total number of days at each station). The aforementioned spatial pattern of concentration around the city center is also visible in Figure 13, where a PM₁₀ exceedance is up to 12 times more probable under a heat wave than a normal day.

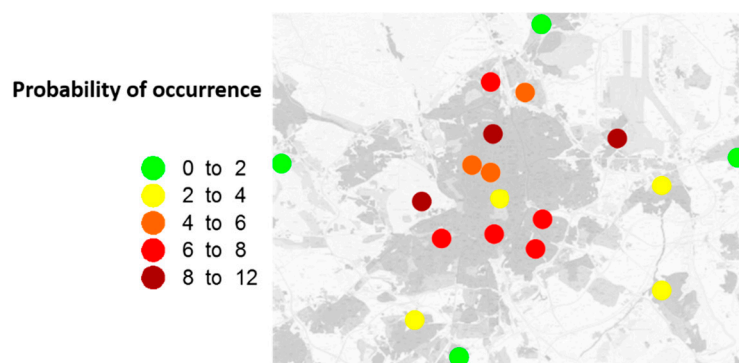


Figure 13. Probability (%) of occurrence of a PM₁₀ exceedance day during a HWD with respect to normal summer days.

Figure 14 verifies the degradation of air quality during HWDs by means of PI in three selected stations: Aguirre (urban traffic), Farolillo (urban background), and Casa de Campo (suburban background). PI values were exclusively determined by PM₁₀ concentrations. Figure 14 shows a clear shift to higher PI classes during HWD, which is more pronounced at the urban traffic station.

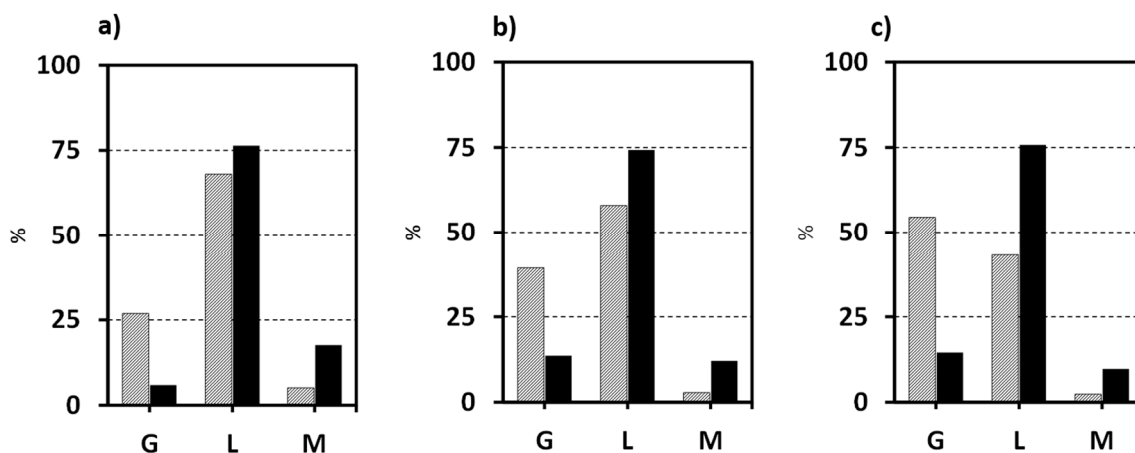


Figure 14. Frequency of occurrence of PI classes (G: good air quality; L: low air quality; M: moderate air quality) during HWDs (solid black bar) and normal summer days (grey bar) at three selected air pollution stations: (a) Aguirre, urban traffic; (b) Farolillo, urban background; and (c) Casa de Campo, suburban background.

As discussed above, we hypothesized the advection of warm air masses from Northern Africa as the most probable cause of heat waves in Madrid. Saharan dust plumes are one the main origins of elevated concentrations of PM₁₀ in Madrid [62,63]. For that reason, we assessed the relationship between heat waves, Saharan dust outbreaks, and air quality conditions in Madrid (Table 4). More Saharan dust outbreaks are expected to occur simultaneously with heat waves (X^2 value of 47.81, significant at 0.001 level); outbreaks simultaneous with heat waves more probably produce a widespread occurrence of PM₁₀ exceedances, as shown by the average ratio between stations with/without exceedances.

Table 4. Combined probability of occurrence of heat wave days and Saharan dust outbreak days (2010–2017) and significance according to an X^2 test.

	Non Outbreak Days	Saharan Outbreak Days
Non heat wave days	486	233
Heat waves days	20	54
Chi-Square test		47.81 *
Stations experiencing PM ₁₀ daily exceedances (% of the total)	28.65	51.53

* Significant at 0.001.

4. Discussion and Conclusions

We analyzed the evolution of heat waves in Madrid (Spain) and their impacts on human comfort. Those extreme events show an increase in frequency and duration after 1980, in close agreement with similar findings about the temporal evolution of heat waves in the Iberian Peninsula and the Mediterranean region [64–70]. Regarding the underlying cause of this trend, it might be primarily related to the increase in global temperatures. However, it is not possible to rule out a regional component in the form of a change in atmospheric circulation, which might favor a higher frequency of hot air masses advectations from southern latitudes. Confirmation of these hypotheses pends future work.

An intensification of the nocturnal CLUHI due to heat waves was identified from the analysis of summer daily temperatures in Madrid, but there is no general agreement so far on the directions of the UHI response to warmer conditions. Some studies report an intensification of the nocturnal UHI during extreme hot days [71–74]; others report a slight intensification of both daytime and nighttime UHI [75], or even a simple modification of the diurnal spatial pattern of the UHI [39]. Some studies found no intensification of the nocturnal UHI during heat waves [21,76]. Additional discussions have arisen about the physical mechanisms that might enhance the nocturnal UHI during heat waves. Whereas lack of surface moisture and low winds are usually considered candidates that boost the impact of heat waves on UHI intensity, recent research argues the existence of a cascade of synergetic reactions, with diverse responses depending on the regional climate, location, mesoscale mechanisms, and urban structure [77–79]. The possible enhancement of the nocturnal CLUHI under warmer conditions has profound implications, but simulations of the magnitude of the CLUHI under the global warming also produced divergent results [80–82].

Worldwide, the SUHI varies considerably depending on urban density, surface properties, extent of vegetation, etc. [83–85]. Madrid, as the majority of cities, experiences a well-developed nocturnal SUHI, whereas its diurnal SUCI is not as frequent [86,87]. The structure of the nocturnal pattern displays higher values in the city center and a sharp gradient in the western part of the city, which occurs due to the predominance of forests and a concave topography. By day, the rural surfaces, mostly occupied by dry farming fields or scrublands under sandy or gypsum soils, experience extreme warming that reverses the urban-to-rural thermal contrast, generating a SUCI, whereas aquatic surfaces become the most significant cooling sources [88]. Under heat wave conditions, both the diurnal SUCI and the nocturnal SUHI intensify, but the magnitudes are not symmetrical, since the average value of the former is about 1 °C and the latter 2 °C.

Regarding the impact of urban spaces on human comfort, a diurnal intensification of the heat stress in the city during the daytime, using the Physiological Equivalent Temperature, was found. The nocturnal physiological heat island is less intense than its nocturnal air temperature counterpart. Two explanations are possible:

(1) The 00 UTC synoptic observation does not represent the maximum intensity of the summer urban heat island, since sunset occurred just a few hours prior and the differential cooling of the countryside is beginning.

(2) During daytime, high air temperatures, dry conditions, and strong solar radiation—the basic elements of the extreme diurnal heat stress in Madrid—are approximately the same in the city (Madrid-Retiro) and the suburban areas (Barajas, Cuatro Vientos, Getafe, and Torrejón de Ardoz). However, there is a substantial contrast regarding wind speeds. Convective movement derived from the strong surface warming should enhance the turbulent mixing in the lower levels of the troposphere, leading to higher wind speeds in the suburban areas (3.6 m·s⁻¹ on average), whereas buildings slow down the wind (2.1 m·s⁻¹ on average) in the urban weather station. Consequently, a slight refreshing effect is experienced in the suburban areas. During nighttime, the stable layer in the suburban areas reduces the wind speed, so differences in PET between urban and non-urban observatories are weaker.

Finally, we highlighted the coincidence between heat waves, strong nocturnal urban heat islands, and worsening of the air quality in the Madrid city center due to rising levels of PM₁₀. This is not surprising due to the common African origin of some, but not all, air masses. Some HWD are accompanied by an autochthonous high dust atmospheric load, when, under large-scale atmospheric stagnation conditions, the poor vegetal cover, a dry environment (low precipitation, high radiation intakes), and the warming of unprotected soils, a strong low tropospheric convection develops, favoring the resuspension of crustal or soil particles [89].

Excessive nocturnal heat negatively influences not only human health—including increasing mortality rates due to heat stress [90,91] and more frequent insomnia [92]—but also impacts labor productivity [93]. Many analyses have highlighted the vulnerability of Madrid's population to extreme temperatures; likewise, both mortality and morbidity are closely related to the worsening of air quality

in the city [94–96]. Besides, research has shown a distinctive spatial pattern of mortality: the city center districts are more vulnerable because of the predominance of aged people, and the antiquity and lower quality of the buildings [97]. Our research agrees with this pattern of vulnerability, since those districts experience an enhanced nocturnal UHI and the worst air quality during heat waves. Thus, as recently developed at the national scale [98], the implementation of prevention plans designed to minimize the impact of high temperatures on health should include the impact of the higher nocturnal urban temperatures, resulting from urban heat islands, to reduce the effect of heat waves on population health. This action should be accompanied by studies analyzing the spatial and temporal variability of urban heat islands at finer scales.

Author Contributions: D.R. and F.F. conceived and designed the study; D.R., F.A., A.M., and F.F. conducted the research, analyzed the data and wrote the paper.

Funding: This research was funded by the research project number CGL2016-80154-R “Análisis y modelización de eventos climáticos extremos en Madrid: olas de calor e inversiones térmicas” funded by Convocatoria 2016 de Proyectos de I+D+I, correspondientes al programa estatal de Investigación, Desarrollo e Innovación Orientada a los Retos de la Sociedad, from the Spanish Ministry of Education.

Acknowledgments: We acknowledge AeMet (Spanish Meteorological Agency) for the cession of meteorological data, Ayuntamiento de Madrid y Comunidad Autónoma de Madrid for the air pollution data, and NASA for the MODIS images at <https://modis.gsfc.nasa.gov/data/dataproduct/mod11.php>. We acknowledge A. Matzarakis for the Rayman software, which can be freely download at <https://www.urbanclimate.net/rayman/>. We thank I. Stewart for help in classifying the Madrid-Retiro and Barajas stations.

Conflicts of Interest: The authors declare no conflict of interest.

References

- Schär, C.; Vidale, P.L.; Luthi, D.; Frei, C.; Haberli, C.; Liniger, M.A.; Appenzeller, C. The role of increasing temperature variability in European summer heat waves. *Nature* **2004**, *427*, 332–336. [CrossRef] [PubMed]
- Zampieri, M.; Russo, S.; Di Sabatino, S.; Michetti, M.; Scoccimarro, E.; Gualdi, S. Global assessment of heat wave magnitudes from 1901 to 2010 and implications for the river discharge of the Alps. *Sci. Total Environ.* **2016**, *571*, 1330–1339. [CrossRef]
- Meel, G.A.; Tebaldi, C. More Intense, more frequent, and longer lasting heat waves in the 21st century. *Science* **2004**, *305*, 994–997. [CrossRef]
- Tebaldi, C.; Hayhoe, K.; Arblaster, J.M.; Meehl, G.A. Going to extremes. *Clim. Chang.* **2006**, *79*, 185–211. [CrossRef]
- Gedzelman, S.D.; Austin, S.; Cermak, R.; Stefano, N.; Partridge, S.; Quesenberry, S.; Robinson, D.A. Mesoscale aspects of the Urban Heat Island around New York City. *Theor. Appl. Climatol.* **2003**, *75*, 29–42.
- Lokoshchenko, M.A. Urban ‘heat island’ in Moscow. *Urb. Clim.* **2014**, *10*, 550–562. [CrossRef]
- Wilby, R. Past and projected trends in London’s urban heat island. *Weather* **2006**, *58*, 251–260. [CrossRef]
- Oke, T.R. The energetic basis of the urban heat island. *Q. J. R. Met. Soc.* **1982**, *108*, 1–24. [CrossRef]
- Arnfield, A.J. Two decades of urban climate research: A review of turbulence, exchanges of energy and water, and the urban heat island. *Int. J. Climatol.* **2003**, *23*, 1–26. [CrossRef]
- Basu, R.; Samet, J.M. Relation between elevated ambient temperature and mortality: A review of the epidemiologic evidence. *Epidemiol. Rev.* **2002**, *24*, 190–202. [CrossRef]
- Conti, S.; Meli, P.; Minelli, G.; Solimini, R.; Toccaceli, V.; Vichi, M.; Beltrano, C.; Perini, L. Epidemiologic study of mortality during the summer 2003 heat wave in Italy. *Environ. Res.* **2005**, *98*, 390–399. [CrossRef]
- Tan, J.; Zheng, Y.; Tang, X.; Guo, C.; Li, L.; Song, G.; Zhen, X.; Yuan, D.; Kalkstein, A.J.; Chen, H. The urban heat island and its impact on heat waves and human health in Shanghai. *Int. J. Biometeorol.* **2010**, *54*, 101–112. [CrossRef]
- Smid, M.; Russo, S.; Costa, A.C.; Granell, C.; Pebesma, E. Ranking European Capitals by Exposure to Heat Waves and Cold Waves. *Urban. Clim.* **2019**, *27*, 388–402. [CrossRef]

14. Kovats, R.S.; Valentini, R.; Bouwer, L.M.; Georgopoulou, E.; Jacob, D.; Martin, E.; Rounsevell, M.; Soussana, J.-F. Europe. In *Climate Change 2014: Impacts, Adaptation, and Vulnerability Part B: Regional Aspects. Contribution of Working Group II to the Fifth Assessment Report of the Intergovernmental Panel on Climate Change*; Barros, V.R., Field, C.B., Dokken, D.J., Mastrandrea, M.D., Mach, K.J., Bilir, T.E., Chatterjee, M., Ebi, K.L., Estrada, Y.O., Genova, R.C., et al., Eds.; Cambridge University Press: Cambridge, UK; New York, NY, USA, 2014; pp. 1267–1326.
15. Scortichini, M.; De Sario, M.; de’Donato, F.K.; Davoli, M.; Michelozzi, P.; Stafoggia, M. Short-Term Effects of Heat on Mortality and Effect Modification by Air Pollution in 25 Italian Cities. *Int. J. Environ. Res. Public Health* **2018**, *15*, 1771. [[CrossRef](#)]
16. Tomlinson, C.J.; Chapman, L.; Thornes, J.E.; Baker, C.J. Including the urban heat island in spatial heat health risk assessment strategies: A case study for Birmingham, UK. *Int. J. Health. Geogr.* **2011**, *10*. [[CrossRef](#)]
17. Rizwan, A.; Dennis, L.; Liu, C. A review on the generation, determination and mitigation of Urban Heat Island. *J. Environ. Sci.* **2008**, *20*, 120–128. [[CrossRef](#)]
18. Mills, G. Urban climatology: History, status and prospects. *Urban. Clim.* **2014**, *10*, 479–489. [[CrossRef](#)]
19. Stewart, I.D. A systematic review and scientific critique of methodology in modern urban heat island literature. *Int. J. Climatol.* **2011**, *31*, 200–217. [[CrossRef](#)]
20. Laaidi, K.; Zeghnoun, A.; Dousset, B.; Bretin, P.; Vandentorren, S.; Giraudet, E.; Beaudeau, P. The Impact of heat Islands on Mortality in Paris during the August 2003 Heat Wave. *Environ. Health Perspect.* **2012**, *120*, 254–259. [[CrossRef](#)]
21. Lehoczky, A.; Sobrino, J.A.; Skoković, D.; Aguilar, E. The Urban Heat Island Effect in the City of Valencia: A Case Study for Hot Summer Days. *Urban Sci.* **2017**, *1*, 9. [[CrossRef](#)]
22. Cheval, S.; Dumitrescu, A. The summer surface urban heat island of Bucharest (Romania) retrieved from MODIS images. *Theor. Appl. Climatol.* **2015**, *121*, 631–640. [[CrossRef](#)]
23. Mendelsohn, R.; Kurukulasuriya, P.; Basist, A.; Kogan, F.; Williams, C. Climate analysis with satellite versus weather station data. *Clim. Chang.* **2007**, *81*, 71–83. [[CrossRef](#)]
24. Fanger, P.O. *Thermal Comfort*; McGraw-Hill: New York, NY, USA, 2008.
25. Koppe, C.; Kovats, S.; Jendritzky, G.; Menne, B. Heat-Waves: Risks and Responses. In *Health and Global Environmental Change*; WHO Series N° 2; WHO: Copenhagen, Denmark, 2004; 123p. Available online: <http://www.euro.who.int/en/publications/abstracts/heat-waves-risks-and-responses> (accessed on 5 November 2018).
26. Höppe, P.R. Heat balance modelling. *Experientia* **1993**, *49*, 741–745. [[CrossRef](#)]
27. VDI. *Methods for the Human-Biometeorological Assessment of Climate and Air Hygiene for Urban and Regional Planning. Part I: Climate*; VDI Guideline 3787; Beuth/Verlag: Berlin, Germany, 1998; Available online: https://www.vdi.eu/guidelines/vdi_3787_blat_2-umweltmeteorologie_methoden_zur_human_biometeorologischen_bewertung_von_klima_und_lufthygiene/ (accessed on 5 November 2018).
28. Kalisa, E.; Fadlallah, S.; Amani, M.; Nahayo, L.; Habiyaremye, G. Temperature and air pollution relationship during heatwaves in Birmingham, UK. *Sustain. Cities Soc.* **2018**, *43*, 111–120. [[CrossRef](#)]
29. Schnell, J.L.; Prather, M.J. Co-occurrence of extremes in surface ozone, particulate matter, and temperature over eastern North America. *Proc. Natl. Acad. Sci. USA* **2017**, *114*, 2854–2859. [[CrossRef](#)]
30. Zhang, H.; Wang, Y.; Park, T.; Deng, Y. Quantifying the relationship between extreme air pollution events and extreme weather events. *Atmos. Res.* **2017**, *188*, 64–79. [[CrossRef](#)]
31. Kerr, G.H.; Waugh, D.W. Connections between summer air pollution and stagnation. *Environ. Res. Lett.* **2018**, *13*, 084001. [[CrossRef](#)]
32. Wang, Y.; Xie, Y.; Cai, L.; Dong, W.; Zhang, Q.; Zhang, L. Impact of the 2011 southern US drought on ground-level Fine aerosol concentration in summertime. *J. Atmos. Sci.* **2015**, *72*, 1075–1093. [[CrossRef](#)]
33. Wang, Y.; Xie, Y.; Dong, W.; Ming, Y.; Wang, J.; Shen, L. Adverse effects of increasing drought on air quality via natural processes. *Atmos. Chem. Phys.* **2017**, *17*, 12827–12843. [[CrossRef](#)]
34. INE. Cifras Oficiales de Población Resultantes de la Revisión del Padrón Municipal a 1 de Enero. Available online: <https://www.ine.es/jaxiT3/Datos.htm?t=2881> (accessed on 5 October 2018).
35. Dirección General de Tráfico. Available online: <http://www.dgt.es/es/seguridad-vial/estadisticas-e-indicadores/parque-vehiculos/tablas-estadisticas/2017/> (accessed on 25 November 2018).

36. Ayuntamiento de Madrid. Available online: <https://www.madrid.es/portales/munimadrid/es/Inicio/El-Ayuntamiento/Estadistica/Areas-de-informacion-estadistica/Trafico-transportes-y-comunicaciones/Intensidad-trafico/Intensidad-del-trafico/?vgnnextfmt=default&vgnnextoid=b3c644c95c9b8210VgnVCM2000000c205a0aRCRD&vgnnextchannel=b355bc87e8986210VgnVCM2000000c205a0aRCRD> (accessed on 25 November 2018).
37. Brunet, M.; Saladié, O.; Jones, P.; Sigró, J.; Aguilar, E.; Moberg, A.; Lister, D.; Walther, A.; Almarza, C. The development of a new dataset of Spanish Daily Adjusted Temperature Series (SDATS) (1850–2003). *Int. J. Climatol.* **2006**, *26*, 1777–1802. [[CrossRef](#)]
38. Pongracz, R.; Bartholy, J.; Dezso, Z. Remotely sensed thermal information applied to urban climate analysis. *Adv. Space Res.* **2006**, *37*, 2191–2196. [[CrossRef](#)]
39. Cheval, S.; Dumitrescu, A.; Bell, A. The urban heat island of Bucharest during the extreme high temperatures of July 2007. *Theor. Appl. Climatol.* **2009**, *97*, 391–401. [[CrossRef](#)]
40. Hung, T.; Uchiyama, D.; Ochi, S.; Yasuoka, Y. Assessment with satellite data of the urban heat island effects in Asian mega cities. *Int. J. App. Earth. Obs. Geoinf.* **2006**, *8*, 34–48. [[CrossRef](#)]
41. Wan, Z.; Zhang, Y.; Zhang, Y.Q.; Li, Z.L. Quality assessment and validation of the global land surface temperature. *International. J. Remote Sens.* **2004**, *25*, 261–274. [[CrossRef](#)]
42. Rigo, G.; Parlow, E.; Oesch, D. Validation of satellite observed thermal emission with in-situ measurements over an urban surface. *Remote Sens. Environ.* **2006**, *104*, 201–210. [[CrossRef](#)]
43. European Commission, Joint Research Center. Available online: <http://forobs.jrc.ec.europa.eu/products/glc2000/glc2000.php> (accessed on 1 December 2018).
44. Portal Abierto de Datos. Ayuntamiento de Madrid. Available online: <https://datos.madrid.es/portal/site/egob/menuitem.c05c1f754a33a9fbc4b2e4b284f1a5a0/?vgnnextoid=f3c0f7d512273410VgnVCM2000000c205a0aRCRD&vgnnextchannel=374512b9ace9f310VgnVCM100000171f5a0aRCRD&vgnnextfmt=defaultURL> (accessed on 16 January 2019).
45. Red de Calidad del Aire de la Comunidad de Madrid. Available online: https://gestionamadrid.org/azul_internet/html/web/InformExportacionAccion.icm?ESTADO_MENU=8 (accessed on 16 January 2019).
46. Histórico de Informes de Episodios Naturales. Available online: <https://www.miteco.gob.es/es/calidad-y-evaluacion-ambiental/temas/atmosfera-y-calidad-del-aire/calidad-del-aire/evaluacion-datos/fuentes-naturales/anuales.aspx> (accessed on 16 January 2019).
47. Stewart, I.D.; Oke, T.R. Local Climate Zones for urban temperature studies. *Bull. Am. Meteorol. Soc.* **2012**, *93*, 1879–1900. [[CrossRef](#)]
48. Russo, S.; Sillmann, J.; Fischer, E.M. Top ten European heatwaves since 1950 and their occurrence in the coming decades. *Environ. Res. Lett.* **2015**, *10*, 124003. [[CrossRef](#)]
49. Díaz, J.L.; García-Herrera, R.; Trigo, R.M.; Linares, C.; Valente, M.A.; De Miguel, J.M.; Hernández, E. The impact of the summer 2003 heat wave in Iberia: How should we measure it? *Int. J. Biometeorol.* **2006**, *50*, 159–166. [[CrossRef](#)]
50. Montero, J.C.; Miron, I.J.; Criado, J.J.; Linares, C.; Díaz, J. Difficulties of defining the term, “heat wave”, in public health. *Int. J. Environ. Health Res.* **2013**, *23*, 377–379. [[CrossRef](#)]
51. Díaz, J.L.; Jordán, A.; García, R.; López, C.; Alberdi, J.C.; Hernández, E.; Otero, A. Heat waves in Madrid 1986–1997: Effects on the health of the elderly. *Int. Arch. Occup. Environ. Health* **2002**, *75*, 163–170. [[CrossRef](#)]
52. García-Herrera, R.; Díaz, J.; Trigo, R.M.; Hernández, F. Extreme summer temperatures in Iberia: Health impacts and associated synoptic conditions. *Ann. Geophys.* **2005**, *23*, 239–251. [[CrossRef](#)]
53. Linares, C.; Díaz, J. Impact of high temperatures on hospital admissions: Comparative analysis with previous studies about mortality (Madrid). *Eur. J. Public Health* **2008**, *18*, 317–322. [[CrossRef](#)] [[PubMed](#)]
54. ETCCDI Core Climate Indices. Available online: <http://www.climdex.org/indices.html> (accessed on 15 January 2018).
55. Höppe, P. The physiological equivalent temperature—A universal index for the biometeorological assessment of the thermal environment. *Int. J. Biometeorol.* **1999**, *43*, 71–75. [[CrossRef](#)] [[PubMed](#)]
56. Matzarakis, A.; Mayer, H.; Iziomon, M.G. Applications of a universal thermal index: Physiological equivalent temperature. *Int. J. Biometeorol.* **1999**, *43*, 76–84. [[CrossRef](#)]
57. Mayer, H.; Höppe, P. Thermal comfort on man in different urban environments. *Theor. Appl. Climatol.* **1987**, *38*, 43–49. [[CrossRef](#)]
58. Matzarakis, A.; Mayer, H. Heat stress in Greece. *Int. J. Biometeorol.* **1997**, *41*, 34–39. [[CrossRef](#)]

59. Murena, F. Measuring air quality over large urban areas: Development and application of an air pollution index at the urban area of Naples. *Atmos. Environ.* **2004**, *38*, 6195–6202. [[CrossRef](#)]
60. Sánchez-Benítez, A.; García-Herrera, R.; Barriopedro, D.; Sousa, P.M.; Trigo, R.M. The Earliest European Summer Mega-heatwave of Reanalysis Period. *Geophys. Res. Lett.* **2018**, *45*, 1955–1962. [[CrossRef](#)]
61. Peña-Ortiz, C.; Barriopedro, D.; García-Herrera, R. Multidecadal Variability of the Summer Length in Europe. *J. Clim.* **2015**, *28*, 5375–5388. [[CrossRef](#)]
62. Querol, X.; Alastuey, A.; Moreno, T.; Viana, M.M.; Castillo, S.; Pey, J.; Rodríguez, S.; Artiñano, B.; Salvador, P.; Sánchez, M.; et al. Spatial and temporal variations in airborne particulate matter (PM10 and PM2.5) across Spain 1999–2005. *Atmos. Environ.* **2008**, *42*, 3964–3979. [[CrossRef](#)]
63. Salvador, P.; Artiñano, B.; Viana, M.M.; Querol, X.; Alastuey, A.; González-Fernández, I.; Alonso, R. Spatial and temporal variations in PM10 and PM2.5 across Madrid metropolitan area in 1999–2008. *Proc. Environ. Sci.* **2011**, *4*, 198–208. [[CrossRef](#)]
64. Abaurrea, J.; Asín, J.; Cebrián, A.C.; Centelles, A. Modeling and forecasting extreme hot events in the central Ebro valley, a continental-Mediterranean area. *Glob. Planet. Chang.* **2007**, *57*, 43–58. [[CrossRef](#)]
65. Nastos, P.T. and Matzarakis, A. Variability of tropical days over Greece within the second half of the twentieth century. *Theor. Appl. Climatol.* **2008**, *93*, 75–89. [[CrossRef](#)]
66. Shevchenko, O.; Lee, H.; Snizhko, S.; Mayer, H. Long-term analysis of heat waves in Ukraine. *Int. J. Climatol.* **2014**, *34*, 1642–1650. [[CrossRef](#)]
67. Unkašević, M.; Tošić, I. Seasonal analysis of cold and heat waves in Serbia during the period 1949–2012. *Theor. Appl. Climatol.* **2015**, *120*, 29–40. [[CrossRef](#)]
68. Ramos, A.M.; Trigo, R.M.; Santo, F.E. Evolution of extreme temperatures over Portugal: Recent changes and future scenarios. *Clim. Res.* **2011**, *48*, 177–192. [[CrossRef](#)]
69. Kyselý, J. Recent severe heat waves in central Europe: How to view them in a long-term prospect? *Int. J. Climatol.* **2010**, *30*, 89–109. [[CrossRef](#)]
70. Tomczyk, A.M.; Pórolniczak, M.; Bednorz, E. Circulation conditions effect on the occurrence of heat waves in Western and Southwestern Europe. *Atmosphere* **2017**, *8*, 31. [[CrossRef](#)]
71. Li, D.; Bou-Zeid, E. Synergistic interactions between urban heat islands and heat waves: The impact in cities is larger than the sum of its parts. *J. Appl. Meteorol. Climatol.* **2013**, *52*, 2051–2064. [[CrossRef](#)]
72. Li, D.; Sun, T.; Liu, M.; Yang, L.; Wang, L.; Gao, Z. Contrasting responses of urban and rural surface energy budgets to heat waves explain synergies between urban heat islands and heatwaves. *Environ. Res. Lett.* **2015**, *10*, 054009. [[CrossRef](#)]
73. Li, D.; Sun, T.; Liu, M.; Wang, L.; Gao, Z. Changes in wind speed under heat waves enhance urban heat islands in the Beijing Metropolitan Area. *J. Appl. Meteorol. Climatol.* **2016**, *55*, 2369–2371. [[CrossRef](#)]
74. Founda, D.; Pierros, F.; Petrakis, M.; Zerefos, C. Inter-decadal variations and trends of the Urban Heat Island in Athens (Greece) and its response to heat waves. *Atmos. Res.* **2015**, *161–162*, 1–13. [[CrossRef](#)]
75. Schatz, J.; Kucharik, C.J. Urban climate effects on extreme temperatures in Madison, Wisconsin, USA. *Environ. Res. Lett.* **2015**, *10*, 094024. [[CrossRef](#)]
76. Scott, A.; Waugh, D.W.; Zaitchik, B.F. Reduced Urban Heat Island intensity under warmer conditions. *Environ. Res. Lett.* **2018**, *13*. [[CrossRef](#)]
77. Founda, D.; Santamouris, M. Synergies between Urban Heat Island and Heat Waves in Athens (Greece), during an extremely hot summer. *Sci. Rep.* **2017**, *7*, 10973. [[CrossRef](#)]
78. Zhao, I.; Oppenheimer, M.; Zhu, Q.; Baldwin, J.W.; Ebi, K.L.; Bou-Zeid, E.; Guan, K.; Liu, L. Interactions between urban heat islands and heat waves. *Environ. Res. Lett.* **2018**, *13*. [[CrossRef](#)]
79. Zhao, L.; Lee, X.; Smith, R.B.; Oleson, K. Strong contributions of local background climate to urban heat islands. *Nature* **2014**, *511*, 216–219. [[CrossRef](#)]
80. Wilby, R.L. Constructing climate change scenarios of urban heat island intensity and air quality. *Environ. Plan. B Plan. Des.* **2008**, *35*, 902–911. [[CrossRef](#)]
81. Sachindra, D.A.; Ng, A.; Muthukumaran, S.; Perera, B.J.C. Impact of Climate Change on Urban Heat Island Effect and Extreme Temperatures: A Case Study. *Q. J. R. Met. Soc.* **2016**, *142*, 172–186. [[CrossRef](#)]
82. McCarthy, M.P.; Harpham, C.; Goodess, C.M.; Jones, P.D. Simulating climate change in UK cities using a regional climate model, HadRM3. *Int. J. Climatol.* **2011**, *32*, 1875–1888. [[CrossRef](#)]

83. Schwarz, N.; Lautenbach, S.; Seppelt, R. Exploring indicators for quantifying surface urban heat islands of European cities with MODIS land surface temperatures. *Remote Sens. Environ.* **2011**, *115*, 3175–3186. [[CrossRef](#)]
84. Zhou, D.; Zhao, S.; Liu, S.; Zhang, L.; Zhu, C. Surface urban heat island in China's 32 major cities: Spatial patterns and drivers. *Remote Sens. Environ.* **2014**, *152*, 51–61. [[CrossRef](#)]
85. Yang, Q.; Huang, X.; Li, J. Assessing the relationship between surface urban heat islands and landscape patterns across climatic zones in China. *Sci. Rep.* **2017**, *7*, 9337. [[CrossRef](#)]
86. López Gómez, A.; López Gómez, J.; Fernández, F.; Moreno, A. *El Clima Urbano. Teledetección de la isla de Calor en Madrid*; Ministerio de Obras Públicas y Transportes: Madrid, Spain, 1993.
87. Sobrino, J.A.; Oltra-Carrió, R.; Sòria, G.; Jiménez-Muñoz, J.C.; Franch, B.; Hidalgo, C.; Mattar, Y.; Julien, J.C.; Romaguera, M.; Gómez, J.A.; et al. Evaluation of the surface urban heat island effect in the city of Madrid by thermal remote sensing. *Int. J. Remote Sens.* **2013**, *34*, 3177–3192. [[CrossRef](#)]
88. Xiao, H.; Kopecká, M.; Guo, S.; Guan, Y.; Cai, D.; Zhang, C.; Zhang, X.; Yao, W. Responses of Urban Land Surface Temperature on Land Cover: A Comparative Study of Vienna and Madrid. *Sustainability* **2018**, *10*, 260. [[CrossRef](#)]
89. García Herrera, R.; Prieto, L.; Díaz, J.; Hernández, E.; Teso, T. Synoptic conditions leading to extremely high temperatures in Madrid. *Annal. Geophys.* **2002**, *20*, 237–245. [[CrossRef](#)]
90. Gabriel, K.M.A.; Endlicher, W.R. Urban and rural mortality rates during heat waves in Berlin and Brandenburg, Germany. *Environ. Pollut.* **2011**, *159*, 2044–2050. [[CrossRef](#)]
91. Royé, D. The effects of hot nights on mortality in Barcelona, Spain. *Int. J. Biometeorol.* **2017**, *61*, 2127–2140. [[CrossRef](#)]
92. Vineis, P. Climate change and the diversity of its health effects. *Int. J. Public Health* **2010**, *55*, 81–82. [[CrossRef](#)]
93. Zander, K.K.; Botzen, W.J.W.; Oppermann, E.; Kjellstrom, T.; Garnett, S.T. Heat stress causes substantial labour productivity loss in Australia. *Nat. Clim. Chang.* **2015**, *5*, 647–651. [[CrossRef](#)]
94. Díaz, J.; Linares, C.; García-Herrera, R.; López, C.; Trigo, R. Impact of temperature and air pollution on the mortality of children in Madrid. *J. Occup. Environ. Med.* **2004**, *46*, 768–774. [[CrossRef](#)]
95. Díaz, J.; López, A.; Carmona, R.; Mirón, J.; Luna, M.Y.; Linares, C. Short-term effect of heat waves on hospital admissions in Madrid: Analysis by gender and comparison with previous findings. *Environ. Pollut.* **2018**, *243*, 1648–1656. [[CrossRef](#)] [[PubMed](#)]
96. Reyes, M.; Díaz, J.; Tobias, A.; Montero, J.C.; Linares, C. Impact of Saharan dust particles on hospital admissions in Madrid (Spain). *Int. J. Environ. Health Res.* **2014**, *24*, 63–72. [[CrossRef](#)]
97. López-Bueno, J.A.; Díaz, J.; Linares, C. Differences in the impact of heat waves according to urban and peri-urban factors in Madrid. *Int. J. Biometeorol.* **2019**, *63*, 371–380. [[CrossRef](#)]
98. Díaz, J.; Carmona, R.; Mirón, I.J.; Ortiz, C.; León, I.; Linares, C. Geographical variation in relative risks associated with heat: Update of Spain's Heat Wave Prevention Plan. *Environ. Int.* **2015**, *85*, 273–283. [[CrossRef](#)]

